nature neuroscience

YAP and TAZ control peripheral myelination and the expression of laminin receptors in Schwann cells

Yannick Poitelon[1], Camila Lopez-Anido[2], Kathleen Catignas[1], Caterina Berti[1], Marilena Palmisano[1], Courtney Williamson[1], Dominique Ameroso[1], Kansho Abiko[1], Yoonchan Hwang[1], Alex Gregorieff[3], Jeffrey L Wrana[3], Mohammadnabi Asmani[4], Ruogang Zhao[4], Fraser James Sim[5], Lawrence Wrabetz[1,6], John Svaren[2] & Maria Laura Feltri[1,6]

Myelination is essential for nervous system function. Schwann cells interact with neurons and the basal lamina to myelinate axons using known receptors, signals and transcription factors. In contrast, the transcriptional control of axonal sorting and the role of mechanotransduction in myelination are largely unknown. Yap and Taz are effectors of the Hippo pathway that integrate chemical and mechanical signals in cells. We describe a previously unknown role for the Hippo pathway in myelination. Using conditional mutagenesis in mice, we show that Taz is required in Schwann cells for radial sorting and myelination and that Yap is redundant with Taz. Yap and Taz are activated in Schwann cells by mechanical stimuli and regulate Schwann cell proliferation and transcription of basal lamina receptor genes, both necessary for radial sorting of axons and subsequent myelination. These data link transcriptional effectors of the Hippo pathway and of mechanotransduction to myelin formation in Schwann cells.

Mechanical cues are important regulators of cell behavior, and are integrated with biochemical signals to control development, physiology and pathology. Yes-associated protein 1 (Yap) and Taz, two related transcriptional coactivators downstream of the Hippo pathway, are also pivotal for mechanical signal transduction[1]. Upon mechanical or chemical stimulation, Yap and Taz shuttle from the cytoplasm into the nucleus to associate with TEA domain (TEAD) transcription factors and regulate gene expression[2,3]. Whether the Hippo pathway and Yap or Taz are required for myelination is currently unknown. During development, peripheral nerves undergo significant morphogenetic changes that cause mechanical stimulation of Schwann cells interacting with axons and the basal lamina. First, immature Schwann cells separate large axons from axon bundles in a process called radial sorting[4]. After defasciculation, large axons acquire a 1:1 relationship with Schwann cells, which then wrap around the axons to form the myelin sheath. Schwann cells in nerves are also exposed to substantial mechanical stimulation during limb growth and body movement. Finally, in response to injury, Schwann cells change their physical relationship with axons to undergo rapid demyelination and transition to a 'repair' state that is required to clear cell debris, promote axonal regrowth and remyelinate regenerated axons[5]. Thus, mechanotransduction should be critical for nerve development and response to injury, but its molecular mechanisms are poorly understood. In addition, although the network of transcription factors that control myelination has been explored in depth[6], the transcriptional control of radial sorting is largely uncharacterized. Finally, interaction of Schwann cells with the basal lamina during radial sorting is mediated by laminin receptors[7], but what controls their expression is also not known.

We ablated Yap and Taz in Schwann cells. We found that the absence of Yap and Taz caused severe peripheral neuropathy owing to developmental impairment in axonal sorting and that Yap and Taz, presumably with Tead1, are required for the transcriptional regulation of laminin receptors in Schwann cell. Thus, Yap and Taz downstream of mechanotransduction and the Hippo pathway are essential for Schwann cell development.

RESULTS

Activation of Yap and Taz in Schwann cells

Yap and Taz are regulated by the Hippo pathway as well as by mechanotransduction independently of Hippo[1]. Activation of Yap and Taz leads to their retention in the nucleus, where they regulate gene expression to promote proliferation or differentiation, depending on the cell type[8]. To investigate how Yap and Taz are regulated in Schwann cells, we plated rat Schwann cells on dorsal root ganglia (DRG) neurons and monitored Yap and Taz localization in different conditions. Contact with neurons or addition of medium containing ascorbic acid did not activate Yap and Taz, which were found in the cytoplasm of Schwann cells 1 and 3 d after plating (**Fig. 1a**). After 7 d in the presence of ascorbic acid, which causes proliferation, basal lamina deposition and myelination, Yap and Taz were found in

[1]Department of Biochemistry, Hunter James Kelly Research Institute, Jacobs School of Medicine and Biomedical Sciences, State University of New York at Buffalo, Buffalo, New York, USA. [2]Waisman Center, University of Wisconsin–Madison, Madison, Wisconsin, USA. [3]Lunenfeld–Tanenbaum Research Institute, Mount Sinai Hospital, Toronto, Ontario, Canada. [4]Department of Biomedical Engineering, Jacobs School of Medicine and Biomedical Sciences, State University of New York at Buffalo, Buffalo, New York, USA. [5]Department of Pharmacology and Toxicology, Jacobs School of Medicine and Biomedical Sciences, State University of New York at Buffalo, Buffalo, New York, USA. [6]Department of Neurology, Jacobs School of Medicine and Biomedical Sciences, State University of New York at Buffalo, Buffalo, New York, USA. Correspondence should be addressed to M.L.F. (mlfeltri@buffalo.edu).

Received 14 October 2015; accepted 4 May 2016; published online 6 June 2016; doi:10.1038/nn.4316

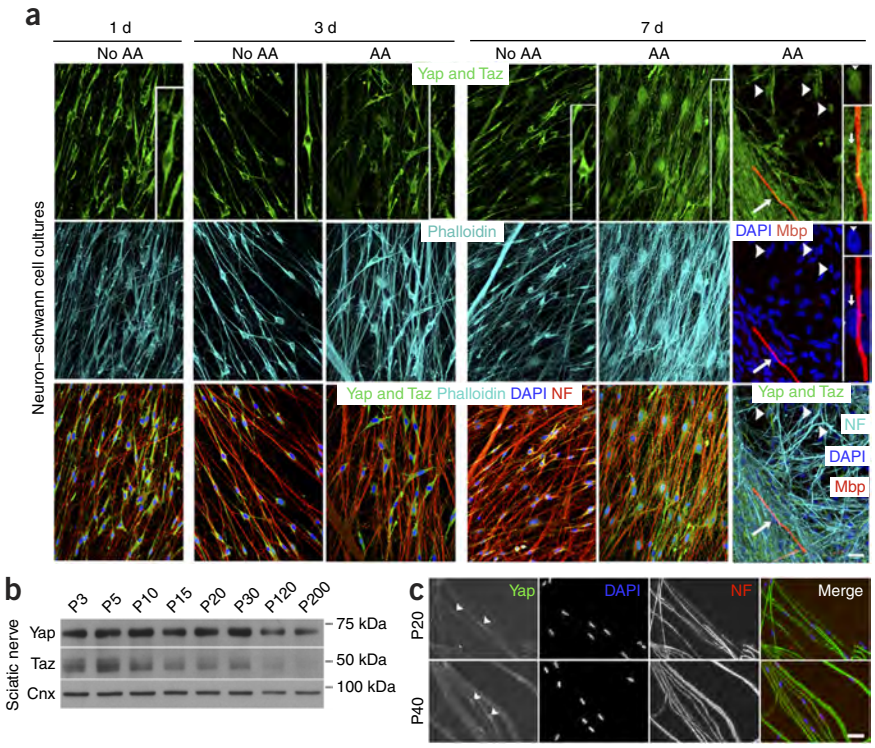

Figure 1 Yap and Taz expression and activation during Schwann cell development. (**a**) Yap and Taz staining (green) of Schwann cells plated on neurons for times indicated in myelinating (ascorbic acid, AA) or nonmyelinating (no AA) conditions. NF, neurofilament staining; DAPI, nuclear staining; phalloidin, F actin staining; Mbp, myelin basic protein. Arrowheads indicate detection of Yap and Taz in the nucleus of Schwann cells at low density; arrows indicate nuclei devoid of Yap and Taz in myelinating Schwann cells. Insets, one cell stained for Yap and Taz in each condition and enlarged. The experiment was repeated twice on at least 3 coverslips per repeat. Scale bar, 20 µm. (**b**) Western blot analysis of Yap and Taz expression during development and myelination in sciatic nerve lysates. Cnx, calnexin. The experiment was performed once (full-length blots are presented in **Supplementary Fig. 4**). (**c**) Teased fibers from P20 and P40 sciatic nerve stained for Yap (green), DAPI (blue) and NF (red) show that Yap is nuclear (arrowheads indicate nuclei) after myelination. The experiment was repeated twice. Scale bar, 20 µm.

the nuclei of many Schwann cells. However, we did not detect Yap or Taz in the nuclei of myelin-forming Schwann cells, indicating that activation of Yap and Taz did not correlate with myelination (**Fig. 1a**). In developing sciatic nerves, Yap and Taz were highly expressed between postnatal day 3 (P3) and P15, when Schwann cells proliferate, sort axons and myelinate, as well as between P15 and P30, during growth and maturation of myelin sheaths, nerves and limbs (**Fig. 1b**). In agreement with those observations, we detected Yap in the nucleus of Schwann cells in sciatic nerves after myelination at P20 and P40 (**Fig. 1c**). Collectively, these data show that Yap and Taz are regulated in developing Schwann cells and suggest a role in myelination. Yap and Taz are activated early during proliferation and basal lamina deposition, and Yap is activated late during myelin maturation and nerve growth, but both Yap and Taz are less activated during active myelin membrane wrapping. This suggests that what distinguishes these situations and determines activation of Yap and Taz is not a specific molecular signal (for example, axonally tethered neuregulin)[9] but rather varying physical stimulation.

Yap and Taz respond to mechanic stimuli in Schwann cells

To determine directly whether Yap and Taz respond to mechanostimulation in Schwann cells, we analyzed their subcellular distribution in response to various modifications of the physical environment. First we used cell density to modify cell geometry. Even when plated without axons, Yap and Taz remained nuclear in Schwann cells spreading at low density but relocated to the cytoplasm in more confluent cultures (**Fig. 2a**). To exclude the possibility that the cytoplasmic localization of Yap and Taz in Schwann cells at higher density was due to Hippo signaling during contact inhibition, we inhibited nonmuscle myosin with blebbistatin, which selectively blocks mechanical Yap and Taz activation independently of the Hippo pathway[1]. In sparse Schwann cell cultures treated with blebbistatin, Yap and Taz remained cytoplasmic (**Fig. 2a**), confirming that the actomyosin cytoskeleton is essential to transduce the mechanical signal that causes Yap and Taz relocalization. We next asked whether Yap and Taz are regulated by substrates of increasing stiffness. We found that both remained cytoplasmic in Schwann cells plated on polyacrylamide hydrogels at elasticity moduli of 0.5 kPa and 40 kPa and on polydimethylsiloxane (PDMS) at 4 MPa (**Fig. 2b**). Only on glass surfaces of extreme stiffness (4 GPa) were Yap and Taz nuclear (**Fig. 1b**). However, when laminin 211 was also coated on the substrates, Yap and Taz moved from cytoplasmic at 0.5 kPa to nuclear at 40 kPa (**Fig. 2c**), both of which are within the physiological range of rigidity[10]. Lastly, we analyzed the localization of Yap and Taz in response to direct mechanical stretching of cells (**Fig. 2d**,**e**). We used a deformable silicone membrane coated with poly-L-lysine or poly-L-lysine plus laminin 211 and stretched Schwann cells for 30 min at 150% static strain. Mechanical stretching with laminin 211 promoted the nuclear localization of Yap and Taz in Schwann cells (**Fig. 2d**,**e**). Taken together, these results show that Yap and Taz are modulated by laminin and mechanical stimuli in Schwann cells.

Taz is required for radial sorting of axons

To determine the function of Yap and Taz in Schwann cells, we generated mice in which one or the other was specifically ablated (**Fig. 3**). Mice bearing *loxP*-flanked *Yap1* or *Wwtr1* (encoding Taz, here referred to as *Taz*)[11] were crossed with P0-Cre mice[12], in which Cre expression is driven in the Schwann cell lineage from embryonic day 13.5 (E13.5) (ref. 13). We found that the resulting *Yap* or *Taz* conditional knockout (cKO) mice showed strong reductions in Yap and Taz expression in sciatic nerves at P20 compared to wild-type controls (**Fig. 3a**). Both *Yap* and *Taz* cKO mice were grossly normal. At P20, cross-sections of sciatic nerves from control littermates showed numerous properly myelinated axons (**Fig. 3b**,**f**,**j**). *Yap* cKO nerves did not show abnormalities of radial sorting or myelination (**Fig. 3c**), whereas *Taz* cKO mice showed many large caliber axons that were not myelinated but grouped in immature bundles (**Fig. 3d**), the hallmark of a partial defect in axonal sorting[7]. Myelin thickness was not significantly affected (**Fig. 3e**). These results indicate that Taz is required for proper sorting of axons by Schwann cells *in vivo*.

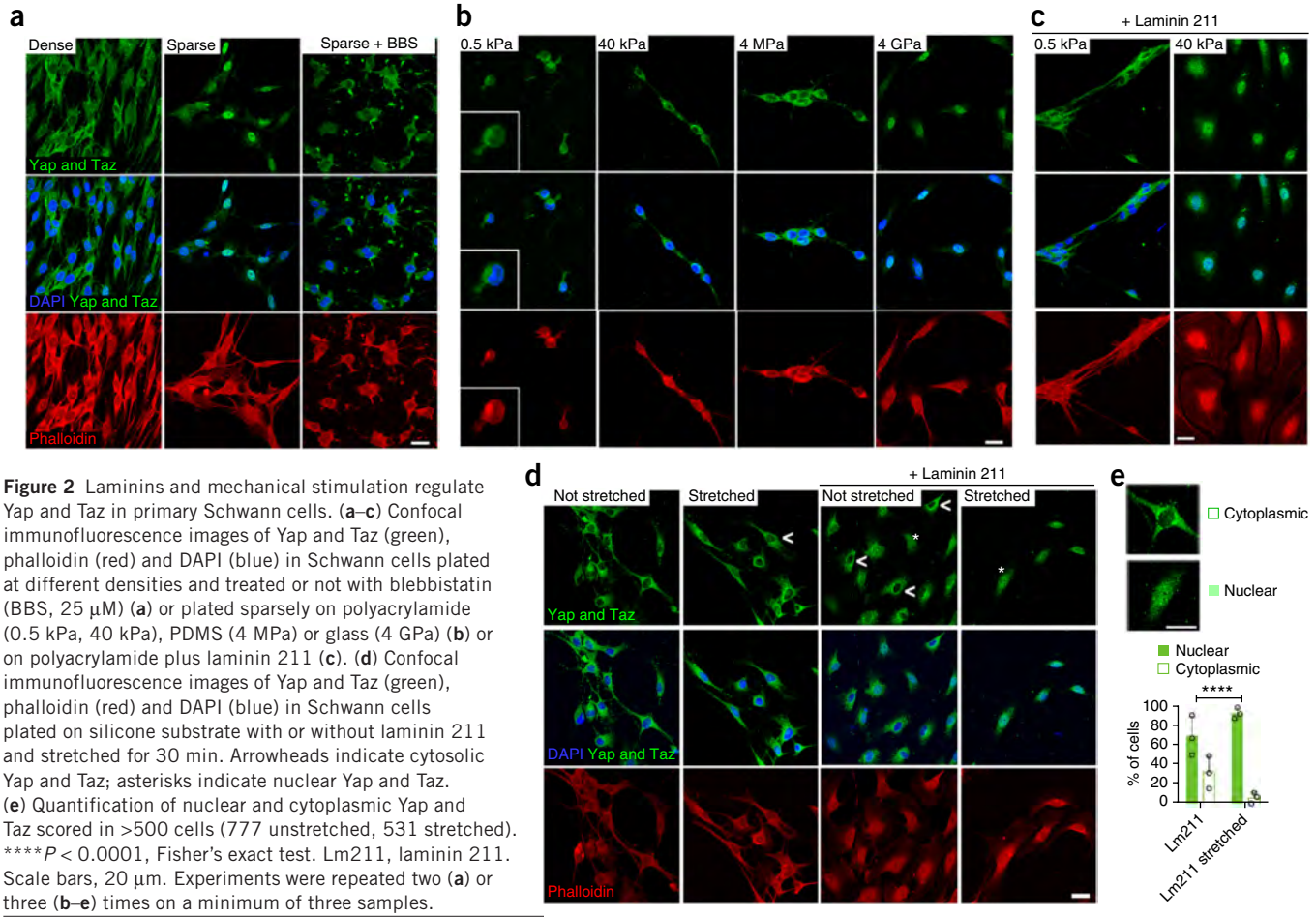

Figure 2 Laminins and mechanical stimulation regulate Yap and Taz in primary Schwann cells. (**a**–**c**) Confocal immunofluorescence images of Yap and Taz (green), phalloidin (red) and DAPI (blue) in Schwann cells plated at different densities and treated or not with blebbistatin (BBS, 25 μM) (**a**) or plated sparsely on polyacrylamide (0.5 kPa, 40 kPa), PDMS (4 MPa) or glass (4 GPa) (**b**) or on polyacrylamide plus laminin 211 (**c**). (**d**) Confocal immunofluorescence images of Yap and Taz (green), phalloidin (red) and DAPI (blue) in Schwann cells plated on silicone substrate with or without laminin 211 and stretched for 30 min. Arrowheads indicate cytosolic Yap and Taz; asterisks indicate nuclear Yap and Taz. (**e**) Quantification of nuclear and cytoplasmic Yap and Taz scored in >500 cells (777 unstretched, 531 stretched). ****$P < 0.0001$, Fisher's exact test. Lm211, laminin 211. Scale bars, 20 μm. Experiments were repeated two (**a**) or three (**b**–**e**) times on a minimum of three samples.

Ablation of Taz and Yap prevents radial sorting

Taz and Yap physically interact and have redundant roles. Taz was upregulated in *Yap* cKO nerves at P20 (**Fig. 3a**), which prompted us to investigate ablation of both Yap and Taz (double cKO). By P20, double-cKO mice showed a severely impaired neuromuscular phenotype with weight loss, muscular atrophy and wide-based gait. By P40, double-cKO mice had nearly paralyzed hind limbs and severe atrophy and were euthanized. Morphological analysis of double-cKO sciatic nerves at P20 revealed a complete arrest in radial sorting; only large bundles of naked axons were present (**Fig. 3i**,**m**), similarly to embryonic nerves. Notably, *Taz* cKO mice heterozygous for *Yap* (Taz cKO–*Yap* cHet) at P20 showed a similar severe external phenotype, with an intermediate morphological phenotype (**Fig. 3g**,**k**,**n**,**o**), with bundles of unsorted axons (**Fig. 3g**,**k**), promyelinating Schwann cells (**Fig. 3g**,**k**) and few myelinated fibers (**Fig. 3g**). In contrast, *Yap* cKO–*Taz* cHet mice did not show a clinical phenotype, and sciatic nerves at P20 showed no radial sorting impairment but did have minor defects, with some Schwann cells blocked at the promyelinating stage (**Fig. 3h**,**l**). Thus, only one allele of *Taz* is sufficient to compensate for *Yap* cKO. Together, these data indicate that Taz has a more prominent role in Schwann cell development and is functionally redundant with Yap in axonal sorting and myelination.

Schwann cell proliferation is reduced in mutant mice

Reduction in number of Schwann cells available to engage axons can impair radial sorting[14]. Failure to generate Schwann cells could be due to defects in proliferation or survival. To verify whether Yap or Taz control Schwann cell proliferation or apoptosis, we measured the fraction of cells positive for phosphorylated histone H3 and TUNEL in P3 sciatic nerves, when matching of the number of Schwann cells and axons by apoptosis, proliferation and radial sorting is ongoing[15]. We focused our analysis on *Taz* cKO–*Yap* cHet mice, as their sciatic nerves showed arrested radial sorting at P20. We first confirmed that the same defect was already present at P3 by semithin section analysis. Indeed, in nerves from wild-type control mice, radial sorting was ongoing and myelination had started, whereas Schwann cells of *Taz* cKO and *Taz* cKO–*Yap* cHet mice were already blocked at an immature stage (**Fig. 4a**,**b**). Only 0.72% of Schwann cells were proliferating in *Taz* cKO–*Yap* cHet sciatic nerves, compared with 2.08% in controls (**Fig. 4c**,**d**). Rates of apoptosis in Schwann cells and density and total number of Schwann cell nuclei were not significantly different between *Taz* cKO–*Yap* cHet and control sciatic nerves, even after taking into account that mutant nerves were smaller and amyelinated, which could increase the density of all cells and mask a reduction of Schwann cell numbers (**Fig. 4c**,**d**). No significant differences in Schwann cell proliferation and apoptosis were detected among all genotypes at P20 after completion of radial sorting (**Supplementary Fig. 1**). However, by P20 the total number of Schwann cells was decreased in double-cKO mice, which were not used for subsequent studies. Thus, the reduction of proliferation in *Taz* cKO–*Yap* cHet Schwann cells might contribute to the severe radial sorting defects.

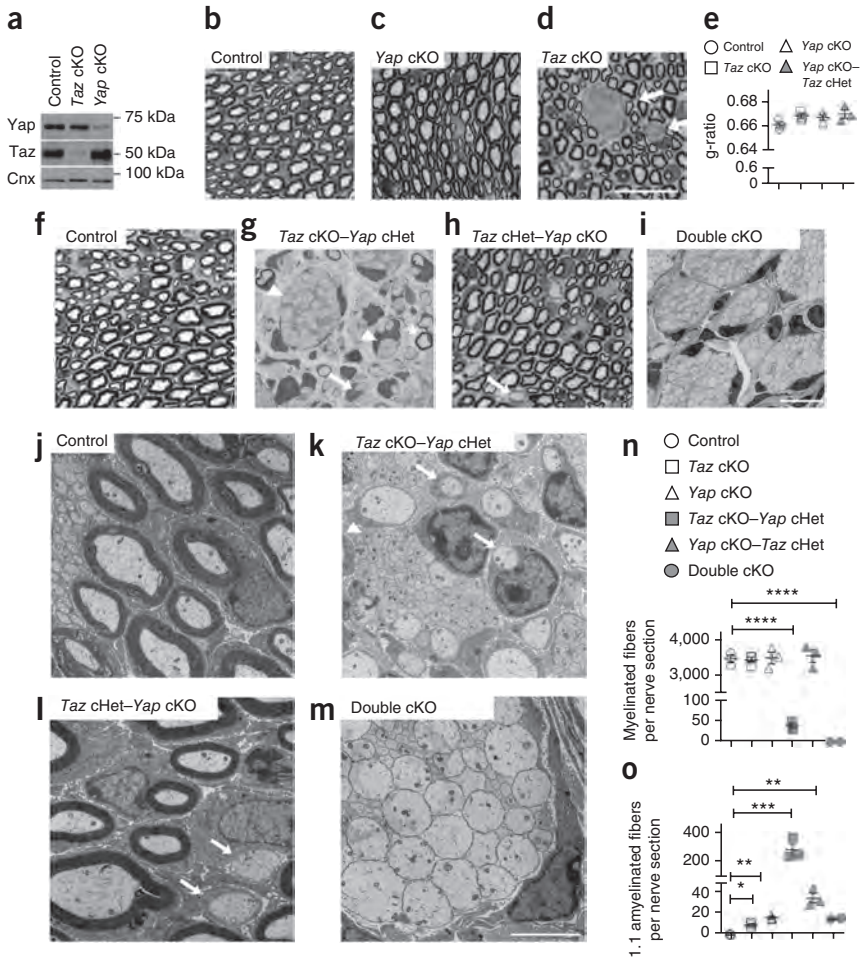

Figure 3 Ablation of Taz in Schwann cells impairs radial sorting of axons. (**a**) Western blot analysis of Taz and Yap expression in sciatic nerves of *Taz* and *Yap* cKO mice. The experiment was repeated twice (full-length blots are presented in **Supplementary Fig. 4**). Cnx, calnexin. (**b**–**d**) Toluidine-blue-stained semithin cross-sections of sciatic nerves from control (**b**) *Yap* cKO (**c**) and *Taz* cKO (**d**) mice at P20. Arrows indicate bundles of unsorted axons. Scale bar, 20 µm. Three mice per genotype were analyzed. (**e**) Myelin thickness as measured by g-ratio in littermate control, Taz cKO, Yap cKO and Yap cKO–Taz cHet mice. Each data point indicates the average value from one nerve from a different animal. Error bars indicate mean and s.e.m. $n = 3$ mice per group. One-way ANOVA. (**f**–**m**) Toluidine-blue-stained semithin cross-sections (**f**–**i**) and electron micrographs (**j**–**m**) of sciatic nerves from control (**f**,**j**), *Taz* cKO–*Yap* cHet (**g**,**k**); *Taz* cHet–*Yap* cKO (**h**,**l**); and double-cKO (**i**,**m**) mice at P20. Scale bars, 10 µm (**b**–**d**), 20 µm (**f**–**i**) or 2 µm (**j**–**m**). Myelinating Schwann cell (asterisks), promyelinating Schwann cells (arrows) and immature Schwann cells (arrowheads) are indicated in **g**, **h**, **k** and **l**. (**n**,**o**) Quantification of myelinated (**n**) and amyelinated (**o**) fibers in control and mutant mice at P20. Data are presented as mean ± s.e.m. Each data point indicates the average value from one nerve from a different mouse; $n = 2$ (double cKO) or 3 mice per genotype (all others). $^{*}P < 0.05$, $^{**}P < 0.01$, $^{***}P < 0.001$, $^{****}P < 0.001$, two-tailed unpaired Student's *t*-test with Bonferroni correction. Detailed statistical information is provided in Online Methods.

Taz and Yap control the expression of laminin receptors

Members of the TEAD family are the main transcription factors that interact with Yap and Taz[3,16]. TEAD binding sites are enriched in enhancers of active genes in peripheral nerves during myelination[17], and TEADs might cooperate with the myelin gene transcription factor Sox10 (ref. 18). We hypothesized that the developmental defects observed in *Taz* cKO mice were caused by a misregulation of TEAD-regulated genes. Using previously published[18] chromatin

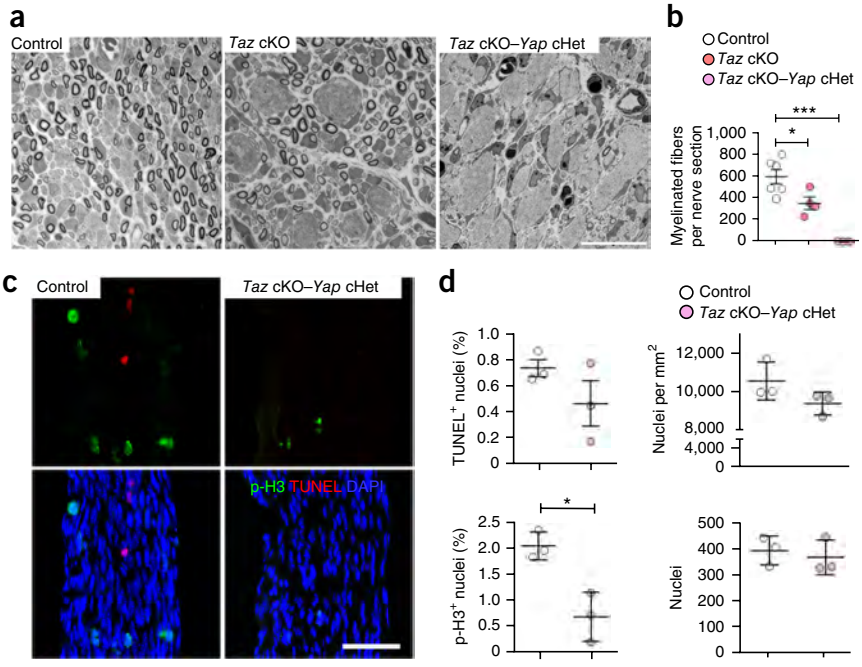

Figure 4 Radial sorting defects in *Taz* cKO–*Yap* cHet nerves are associated with a reduction in Schwann cell proliferation at P3. (**a**) Semithin cross-sections of sciatic nerves stained with Toluidine blue from control, *Taz* cKO and *Taz* cKO–*Yap* cHet mice at P3. Scale bar, 10 µm. $n = 6$ control, 4 *Taz* cKO and 3 *Taz* cKO–*Yap* cHet mice. (**b**) Numbers of myelinated fibers at P3 in control, *Taz* cKO and *Taz* cKO–*Yap* cHet mice. $n = 6$ control, 4 *Taz* cKO and 3 *Taz* cKO–*Yap* cHet mice. (**c**) TUNEL (red) and phosphorylated histone H3 (p-H3) staining (green) and DAPI (blue) analysis on longitudinal section of sciatic nerves from control and *Taz* cKO–*Yap* cHet at P3. Scale bar, 50 µm. $n = 6$ control, 4 *Taz* cKO and 3 *Taz* cKO–Yap cHet mice. (**d**) Relative numbers of TUNEL- and p-H3-positive nuclei and density and total number of nuclei in sciatic nerve (length of sciatic nerve measured = 400 µm). $n = 3$ mice per genotype. Each data point in **b** and **d** indicates the average value from one nerve from one mouse. Error bars indicate mean ± s.e.m. $^{*}P < 0.05$, $^{***}P < 0.001$. Detailed statistical information is provided in Online Methods.

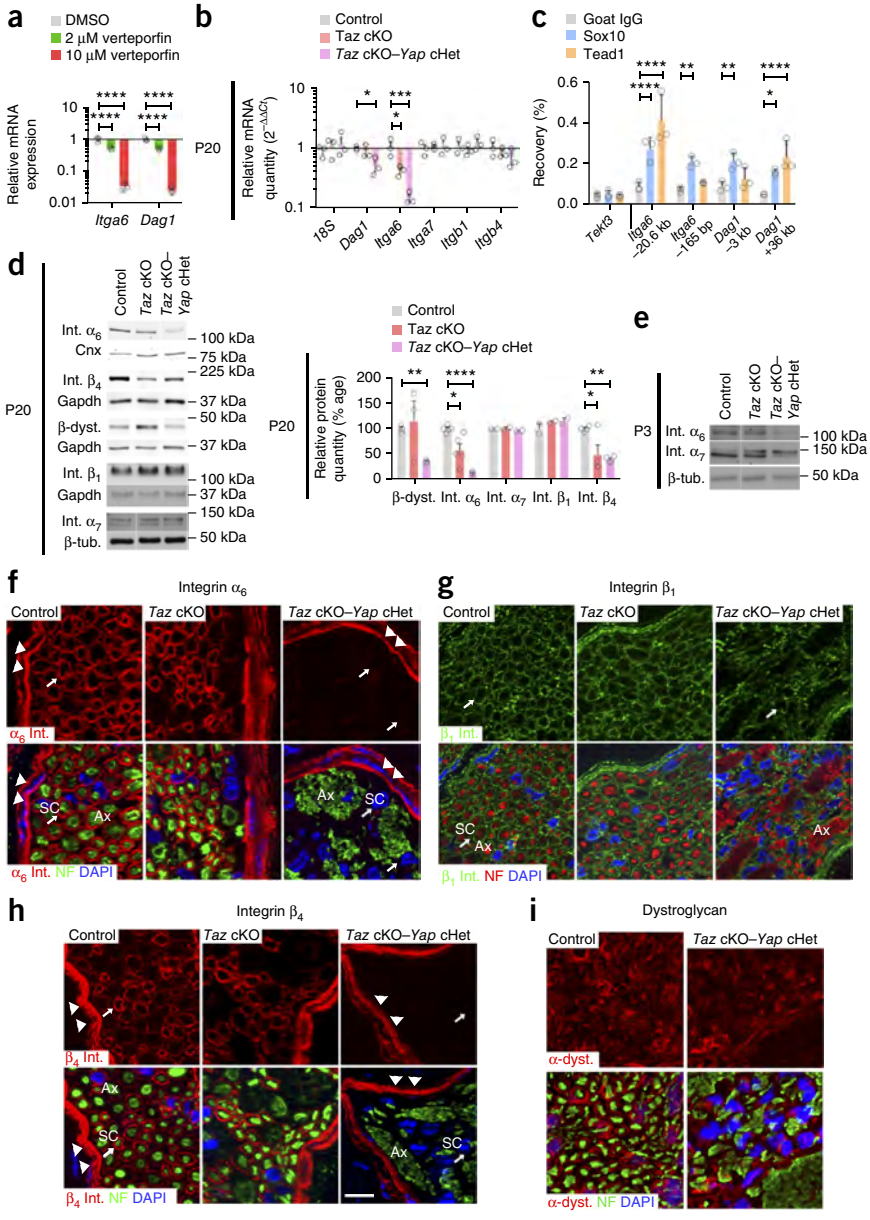

Figure 5 Taz and Yap control expression of integrin α_6 and dystroglycan in Schwann cells. (**a**) mRNA levels of *Dag1* and *Itga6* after verteporfin treatment (relative to DMSO-treated controls) in Schwann cells. $n = 3$ independent experiments with 3 independent samples per group. A logarithmic scale was used for the *y* axis, and the origin was set to 1. (**b**) mRNA expression (relative to wild-type mice) in *Taz* cKO and *Taz* cKO–*Yap* cHet cells at P20. $n =$ 3 mice. A logarithmic scale was used for the *y* axis, and the origin was set to 1. (**c**) ChIP-qPCR analysis of Sox10 and Tead1 binding at *Itga6* and *Dag1* enhancer regions in P15 rat sciatic nerves. Binding was assessed relative to a negative control IP with goat IgG. The negative control is a region 17.8 kb from the *Tekt3* gene, which is not expressed in Schwann cells. $n =$ 3 independent experiments. (**d**,**e**) Western blot analysis (**d** (left) and **e**) and quantification (**d**, right) of integrins and β-dystroglycan (β-dyst.) expression in *Taz* cKO and *Taz* cKO–*Yap* cHet sciatic nerves at P20 (**d**) and P3 (**e**). Cnx, calnexin. For *Dag1*, $n = 3$ mice per group; for *Itga6*, $n = 5$ control and *Taz* cKO and 4 *Taz* cKO–*Yap* cHet mice; for *Itgb4*, $n = 4$ mice per group. (Full-length blots are presented in **Supplementary Fig. 4**.) (**f**–**i**) Localization of integrin α_6 (**f**), β_1 (**g**) and β_4 subunits (**h**) and α-dystroglycan (**i**) in cross-sections of sciatic nerves at P20. Arrowheads indicate integrin α_6 and β_4 subunits (red) around the perineurium; arrows indicate integrin α_6 and β_4 subunits around Schwann cells (SC) in wild-type control nerves; 'ax' indicates axons. Error bars indicate mean ± s.d. (**a**,**c**) or mean ± s.e.m (**b**,**d**); $^*P < 0.05$, $^{**}P < 0.01$, $^{***}P < 0.001$, $^{****}P < 0.0001$, two-way ANOVA with Bonferroni *post hoc* correction (**a**,**c**,**d**) or one-way ANOVA with Bonferroni *post hoc* correction (**b**). Scale bar, 10 μm. Detailed statistical information is provided in Online Methods.

immoprecipitation sequencing (ChIP-seq) data of sciatic nerves, we first identified active enhancers marked by acetylation of histone H3 at Lys27 (H3K27ac) that contained TEAD motifs and were associated with genes controlling Schwann cell development and axonal sorting[18]. Potential TEAD-regulated enhancers were identified for *ErbB2*, *Cdc42*, *Egr2* and *Sox10*, which are involved in the transduction of the axonal signal that guides axonal sorting and myelination[14,19–22] (**Supplementary Fig. 2a**). Treatment of a Schwann cell line with verteporfin, a drug that interferes with Yap–TEAD interactions[23], decreased the expression of *ErbB2*, *Cdc42*, *Egr2* and *Sox10* mRNA (**Supplementary Fig. 2b**). However, we found no *in vivo* evidence of decreased expression of *ErbB2*, *Cdc42* or *Sox10* in mutant sciatic nerves at P20 (**Supplementary Fig. 2c**,**d**). Egr2 protein was also not decreased at P20, but *Egr2* mRNA expression was decreased in *Taz* cKO–*Yap* cHet P3 nerves (discussed below). We then tested regulation of *Itga6*, which encodes an integrin (α_6) that is required for Schwann cells to sort axons[24] and also showed potential TEAD-regulated enhancers (**Supplementary Fig. 3a**). Treatment of primary rat Schwann cells with verteporfin decreased the expression of *Itga6* mRNA (**Fig. 5a**). Notably, mRNA and protein levels of integrin α_6 were reduced in *Taz* cKO and *Taz* cKO–*Yap* cHet mutant sciatic nerves (**Fig. 5b**–**d**) and correlated with the severity of the radial sorting phenotype observed in *Taz* cKO (protein decreased by 59%) and *Taz* cKO–*Yap* cHet (protein decreased by 85%) mutant mice.

To investigate whether TEADs bind directly to *Itga6* regulatory regions, we performed ChIP-qPCR using anti-Tead1, as profiling studies indicate that Tead1 was the most highly expressed TEAD family member in Schwann cells (data not shown). We first performed Tead1-specific ChIP in the rat S16 Schwann cell line, in which *Itga6* expression has been shown to be Sox10 dependent[25]. After testing multiple sites, we found binding of Tead1 at the enhancer 20 kb upstream of *Itga6* (**Supplementary Fig. 3b**). Although the TEAD motif (GGAATG) was not found at this enhancer by HOMER analysis (**Supplementary Fig. 3a**), we found a conserved AGAATG variant, which also binds Tead1 (ref. 26). ChIP-qPCR analysis of P15 sciatic nerves confirmed binding of Tead1 and Sox10 to the same enhancer *in vivo* at −20.6 kb but not to the promoter region bound by Sox10 (**Fig. 5c**).

Deletion of *Itga6* in Schwann cells in mice causes an early and compensatory upregulation of integrin $\alpha_7\beta_1$, requiring ablation of

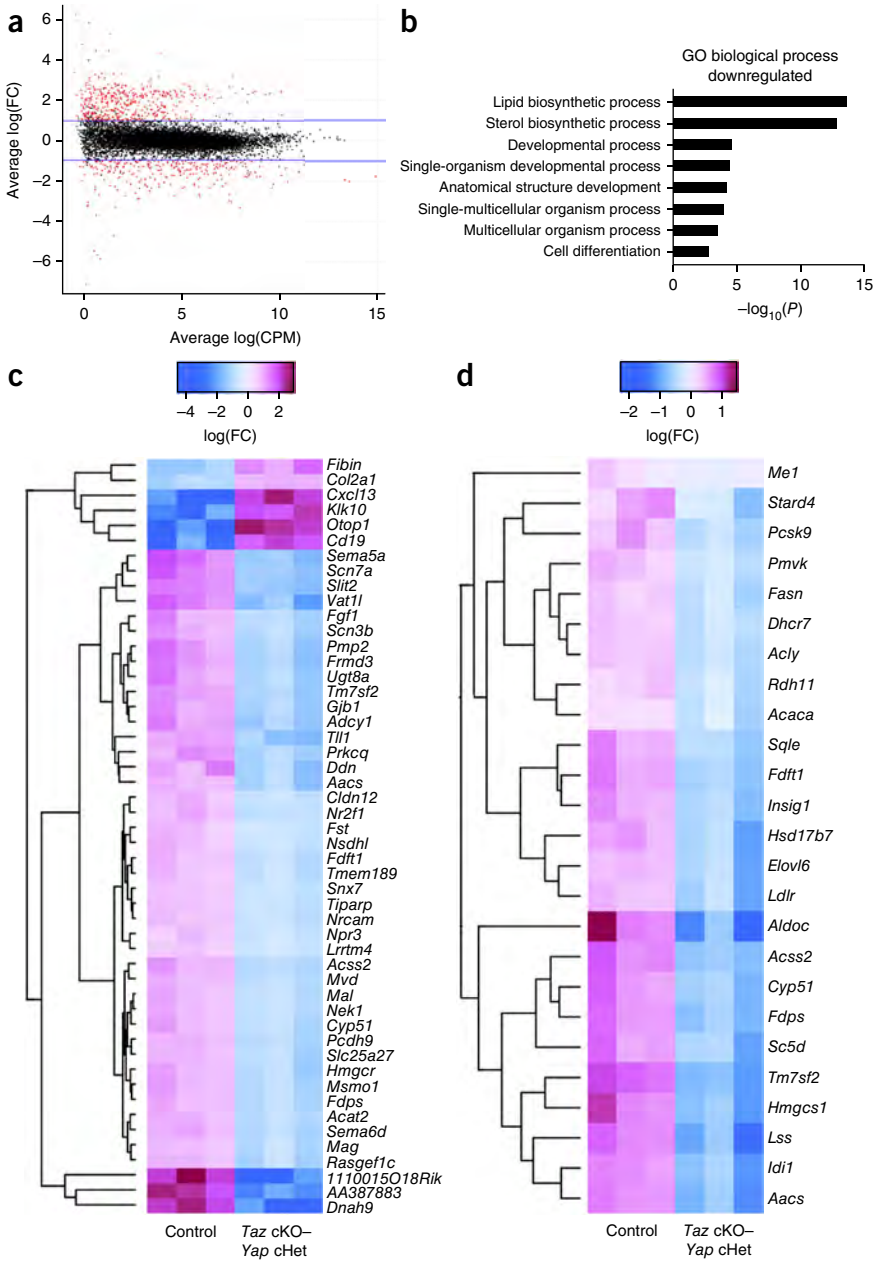

Figure 6 RNA-seq analysis of *Taz* cKO–*Yap* cHet sciatic, brachial and peripheral trigeminal nerves at P3. (**a**) Log_2 fold change (FC) in *Taz* cKO–*Yap* cHet versus control mice plotted against the average count size for every gene. CPM, counts per million. Genes highlighted in red were significantly differentially expressed at 5% false discovery rate (FDR). Blue lines indicate twofold change. (**b**) Gene Ontology analysis of biological processes downregulated significantly in *Taz* cKO–*Yap* cHet mice. (**c**) Heatmap of the top 50 most significant differentially regulated genes. Scale indicates expression relative to median of six samples. (**d**) Heatmap of Srebf target genes (obtained from ref. 31). Scale indicates expression relative to median of six samples. All genes were downregulated in *Taz* cKO–*Yap* cHet mice.

both integrin $\alpha_6\beta_1$ and $\alpha_7\beta_1$ to reveal radial sorting defects[24]. In contrast, in *Taz* cKO and *Taz* cKO–*Yap* cHet cells, the reduction of integrin α_6 was not compensated for by an increase in integrin α_7 at P3 or P20 (**Fig. 5d**,**e**). Staining of sciatic nerve sections confirmed that integrin α_6 was undetectable in *Taz* cKO–*Yap* cHet Schwann cells, whereas its expression was preserved in perineurial cells, in which P0-Cre is not expressed (**Fig. 5f**). The integrin α_6 subunit pairs with integrin β_4 or β_1 subunits to form laminin receptors[27], and previous studies revealed that integrin $\alpha_6\beta_1$ is the relevant receptor in Schwann cells for radial sorting[13,24]. Integrin β_1, which can interact with several other integrin α-subunits in Schwann cells (α_1, α_3, α_5 and α_7)[28], was still present adjacent to the Schwann cell basal lamina in *Taz* cKO–*Yap* cHet nerves (**Fig. 5g**). In contrast, integrin β_4 can dimerize only with the integrin α_6 subunit, and it has been postulated that failed heterodimerization of integrin subunits in the synthetic pathway leads to degradation[27]. In agreement with this idea, we detected no integrin β_4 protein in *Taz* cKO–*Yap* cHet mutant Schwann cells (**Fig. 5h**), despite normal levels of *Itgb4* mRNA (**Fig. 5b**).

Because the *Taz* cKO–*Yap* cHet mutation caused an even more severe phenotype than that seen in the absence of both integrins $\alpha_6\beta_1$ and $\alpha_7\beta_1$ (ref. 24), we asked whether Taz and Yap also control the expression of dystroglycan (encoded by *Dag1*), a third redundant laminin receptor required for radial sorting[29]. We examined two prominent H3K27ac-marked enhancers near *Dag1*, one of which contained a predicted TEAD binding site (**Supplementary Fig. 3a**). Binding of Tead1 to the −36-kb site was detected by ChIP-qPCR *in vivo* using anti-Tead1 (**Fig. 5c**), whereas the other enhancer bound Sox10 but lacked significant Tead1 binding. Verteporfin treatment decreased *Dag1* mRNA (**Fig. 5a**), and mRNA and protein levels for β-dystroglycan were reduced in *Taz* cKO–*Yap* cHet but not *Taz* cKO Schwann cells (**Fig. 5b**,**d**,**i**).

Yap and Taz regulate expression of lipid synthetic enzymes

To examine the function of Yap and Taz in Schwann cells at the genome-wide level, we performed RNA-seq transcriptome profiling of P3 developing peripheral nerves in *Taz* cKO–*Yap* cHet and control mice. We identified 2,076 misregulated transcripts in mutant nerves, 982 of which were increased and 1,093 of whch were decreased at a 5% false discovery rate (**Fig. 6a** and **Supplementary Table 1**). We confirmed that the mRNA for *Itga6* and *Dag1*, as well as the known Yap, Taz and TEAD target genes *Nov* and *Wisp1*, were decreased in in *Taz* cKO–*Yap* cHet mutant nerves. Among the top dysregulated genes were those encoding signaling molecules predicted to be important in nerve development, such as protein kinase C (*Prkcq*) and adenylate cyclase (*Adcy1*); potentially important novel proteins such as the upregulated P2Y receptor inhibitor otopetrin (*Otop1*) and the chemokine Cxcl13 or the downregulated Protocadherin 9 (*Pcdh9*); and the secreted glycoprotein Slit2 (**Fig. 6c**). Genes involved in differentiation, such as *Mag*, *Pmp22* and *Mbp*, were downregulated, and *Sox2* and *Pou3f1*, which are expressed in immature and promyelinating Schwann cells, were upregulated. Notably, we found that the most dysregulated genes encoded lipid and cholesterol biosynthetic and

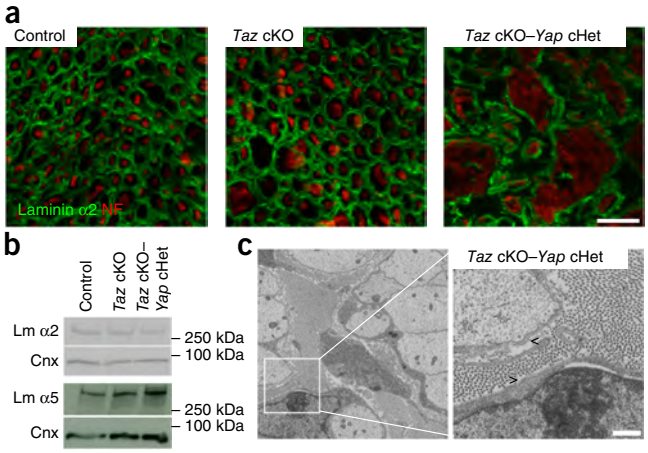

Figure 7 Laminin expression and basal lamina organization in *Taz* cKO and *Taz* cKO–*Yap* cHet nerves. (**a**) Immunolocalization of laminin α2 chain (green) and neurofilament (NF; red) in cross sections of control, *Taz* cKO and *Taz* cKO–*Yap* cHet sciatic nerves at P20. Scale bar, 10 µm. *n* = 2 mice per genotype. (**b**) Western blot analysis of laminin (Lm) α2 and α5 chain expression at P20. *n* = 2 mice per genotype. (full-length blots are presented in **Supplementary Fig. 4**). (**c**) Electron micrographs of *Taz* cKO–*Yap* cHet sciatic nerves at P20. Arrowheads indicate basal lamina properly organized around amyelinated axons. *n* = 1 mouse per genotype. Scale bar, 500 nm. Cnx, calnexin.

regulatory enzymes (**Fig. 6b**,**d**). We performed a gene-set enrichment analysis using the MSigDB C2 database, which contains ~5,000 gene sets[30]. Among genes downregulated in *Taz* cKO–*Yap* cHet mice, we found significant enrichment of sterol regulatory-element-binding protein (Srebf) target genes (gene-set enrichment $P = 5 \times 10^{-4}$)[31] with all 25 genes downregulated in *Taz* cKO–*Yap* cHet mice (**Fig. 6d**). *Srebf2* mRNA itself was reduced by 48.7% in *Taz* cKO–*Yap* cHet cKO mice, compared to controls. A similar decrease of genes involved in lipid biosynthesis and in *Srebf2* was observed in Egr2-deficient mice at P7 (refs. 32,33); therefore, the modest decrease in Egr2 expression may partially account for these observations. Together these data suggest that Yap and Taz are required for normal expression of *Srebf2*, and their deletion substantially impairs the transcription of genes involved in lipid or sterol biosynthesis in Schwann cells.

The basal lamina is preserved in Taz-mutant nerves

Taz regulates the transcription of laminin 511 and the organization of the extracellular matrix in breast cancer cells, and this in turn engages integrins in a positive regulatory loop[34]. Our transcriptomic analysis revealed a reduction of *Lama2* transcripts, which are required to synthesize laminin 211. To determine whether Yap or Taz had a major effect on laminins and the extracellular matrix in our system, we analyzed the expression and localization of laminins and the organization of the Schwann cell basal lamina in control and *Taz* cKO or *Taz* cKO–*Yap* cHet nerves at P20 (**Fig. 7**). Western blot analysis showed that the level of laminin 211 protein was slightly reduced in *Taz* cKO–*Yap* cHet mice (**Fig. 7b**), but we did not find major alterations of laminins or morphological evidence of basal lamina disorganization in mutant mice at this age.

Collectively, our data indicate that Yap, Taz and TEADs regulate the expression of crucial laminin receptors in Schwann cells, namely integrin $\alpha_6\beta_1$, $\alpha_6\beta_4$ and dystroglycan. These defects correlate with the increasing severity in *Taz* cKO and double-cKO mice and, paired with a decrease in Schwann cell proliferation and a defect in lipid biosynthesis, can account for the radial sorting phenotype.

DISCUSSION

We demonstrate that Yap and Taz are required for normal peripheral nerve development. Yap and Taz control radial sorting and subsequent myelination by regulating Schwann cell proliferation and via their role as TEAD transcriptional coactivators. Yap and Taz are redundant in Schwann cells, and mice lacking both *Yap* and *Taz* show complete arrest at the developmental step of axonal sorting. Furthermore, *Yap* is not able to compensate for *Taz* knockout, but one *Taz* allele prevents radial sorting defects in *Yap* cKO–*Taz* cHet mutants.

We identify Yap, Taz and Tead1 as transcriptional regulators of radial sorting in Schwann cells. Radial sorting is a prerequisite for peripheral myelination, as it allows Schwann cells to engage in a 1:1 relationship with a large axon (promyelinating fiber). Although the transcriptional network that controls the transition from pro-myelination to myelination is well established[6], the transcriptional control of radial sorting is poorly understood. Our work places Yap, Taz and Tead1 at the core of the transcriptional regulation of axonal sorting. Unlike Schwann cells, oligodendrocytes in the CNS myelinate multiple axons, and as such do not require a 1:1 relationship to myelinate. In addition, oligodendrocytes do not deposit a basal lamina, and the mechanical stimuli placed on them are likely to be different from Schwann cells[35,36]. Of note, TEAD motifs have been identified in conjunction with Sox10 binding sites in Schwann cells, but not oligodendrocytes[18]. On the basis of these observations, it is tempting to speculate that Yap, Taz and TEADs fulfill different roles in oligodendrocytes and Schwann cells, although this remains to be determined.

We show that laminin-binding integrins and dystroglycan are important downstream targets of Yap, Taz and TEAD transcription. Previous work showed that integrin $\alpha_6\beta_1$ and dystroglycan but not integrin $\alpha_6\beta_4$ are required for radial sorting[7], but the factors that control their expression were unknown. Here we show that Yap and Taz are required for the expression of integrin α_6 and β-dystroglycan in Schwann cells. *Taz* cKO–*Yap* cHet Schwann cells show profound decrease of the major receptors (integrin $\alpha_6\beta_1$, $\alpha_6\beta_4$ and dystroglycan) required to interact with laminins in the basal lamina. Previously work could not assess the independent function of integrin $\alpha_6\beta_1$, as it was compensated for by integrin $\alpha_7\beta_1$ (ref. 24), and deletion of the integrin β_1 subunit in Schwann cells removes 12 integrin receptors[13]. The selective decrease of integrin α_6 subunit in Yap- and Taz-deficient nerves reinforces the idea that integrin $\alpha_6\beta_1$ is the crucial integrin receptor for radial axonal sorting in Schwann cells.

Matching of Schwann cell and axon number is also critical for radial sorting, and mice lacking *Yap* and *Taz* show a decrease of Schwann cell proliferation at P3, which could also contribute to the observed phenotype. This is consistent with the observations that Yap and Taz control cell number and proliferation in a variety of other cell types[37], regulate many cell cycle genes with TEAD and AP1 factors[38] and constitute important checkpoint through the Hippo pathway to neoplastic growth[39].

For ChIP studies we used TEAD binding motifs because they are highly enriched in Schwann-cell-specific enhancers[18], and previous ChIP-seq studies showed that the majority of Yap and Taz sites colocalize with TEAD binding sites. However, Yap and Taz also utilize other partners, such as Runx1 and Runx2, to bind DNA[38], and they can also repress gene expression[40]. Thus, we expect that many genes downstream of Yap and Taz contribute to orchestration of axonal sorting and myelination. To begin to address this issue, we performed genome-wide transcriptomic profiling and found that Yap and Taz

are required for proper expression of many genes, including the network that controls Schwann cell differentiation and myelination. Among these, lipid and sterol synthetic and regulatory genes were particularly affected, including all the targets of *Srebf2*. Whether Yap or Taz directly regulates these genes remains an important question to investigate. Overall, we propose that the combined reduction of dystroglycan and integrin $\alpha_6\beta_1$ without integrin $\alpha_7\beta_1$ compensation, together with the reduction of Schwann cell proliferation and of the cholesterol biosynthesis pathways, represent possible mechanisms by which the phenotype might emerge.

An important question is what controls Yap and Taz activation in Schwann cells. Yap and Taz are downstream of mechanotransduction and the Hippo pathway, which can be activated by multiple upstream inputs, such Wnt, G-coupled-protein receptors, EGF and TGF-β signaling[41]. Some of these pathways are involved in Schwann cell development and could conceivably regulate Yap and Taz in Schwann cells[42–44]. Also, mechanical stimuli such as compression and traction forces exerted by neighboring cells or by the extracellular matrix participate in the activation of Yap and Taz in several cell types[41]. We found that a combination of laminin 211 and mechanical stimuli activate Yap and Taz in Schwann cells; it will be interesting in the future to determine which receptors are involved. Reverse genetic and *in vitro* experiments suggest that Schwann cells respond to basal lamina composition and its mechanical properties during radial sorting and myelination[13,44–47], but the molecular mechanisms are not known. Indeed, we expected that integrins, potential mechanotransducers[48], would lie upstream of Yap and Taz but were surprised to find that they were instead regulated by Yap and Taz. Because laminin 211 acts synergistically with mechanical stimulation to activate Yap and Taz, it is possible that basal lamina components activate Yap and Taz via integrins or Gpr126 in a positive feedback loop[44,49]. Diseases such as hereditary neuropathy with liability to pressure palsy also underscore the importance of physical forces in peripheral myelination, where abla tion of one copy of the gene encoding peripheral myelin protein 22 in Schwann cells causes demyelination after minor mechanical stimuli by largely unknown mechanisms[50]. Thus, mechanotransduction is likely to be critical for nerve development and disease, and our work helps to shed light on its molecular mechanisms.

METHODS

Methods and any associated references are available in the online version of the paper.

Accession codes. Gene Expression Omnibus:, GSE79115.

Note: Any Supplementary Information and Source Data files are available in the online version of the paper.

ACKNOWLEDGMENTS

We thank E. Hurley for technical assistance; A. Sonnenberg (Netherlands Cancer Institute), D. Meijer and P. Brophy (Centre for Neuroregeneration, Edinburgh), the late G. Tarone (University of Turin), L. Sorokin (University of Muenster) and M. Wegner (Friedrich-Alexander University Erlangen–Nürnberg) for antibodies, and the late R. Quarles (National Institute of Neurological Diseases and Stroke) for the S16 cells. This work was funded by grants NS045630 (to M.L.F.), NS096104 (to L.W.) and NS075269 (to J.S.).

AUTHOR CONTRIBUTIONS

Y.P., K.C., C.B., M.P. and M.L.F. designed research and interpreted data; Y.P. performed experiments with assistance from C.L.-A., K.C., C.B., M.P., C.W., D.A., K.A. and Y.H.; C.L.-A. and J.S. designed and performed ChIP sequencing and promoter analysis. M.A. and R.Z. designed and helped to perform biomechanical experiments; A.G. and J.L.W. and L.W. contributed analytical tools; F.J.S. analyzed RNA-seq data; Y.P. and M.L.F. wrote the manuscript; Y.P., C.L.-A., R.Z., F.J.S., J.S., L.W. and M.L.F. analyzed data and critically reviewed the manuscript.

COMPETING FINANCIAL INTERESTS

The authors declare no competing financial interests.

1. Dupont, S. *et al.* Role of YAP/TAZ in mechanotransduction. *Nature* **474**, 179–183 (2011).
2. Zhao, B. *et al.* TEAD mediates YAP-dependent gene induction and growth control. *Genes Dev.* **22**, 1962–1971 (2008).
3. Zhang, H. *et al.* TEAD transcription factors mediate the function of TAZ in cell growth and epithelial-mesenchymal transition. *J. Biol. Chem.* **284**, 13355–13362 (2009).
4. Webster, H.D., Martin, R. & O'Connell, M.F. The relationships between interphase Schwann cells and axons before myelination: a quantitative electron microscopic study. *Dev. Biol.* **32**, 401–416 (1973).
5. Jessen, K.R., Mirsky, R. & Lloyd, A.C. Schwann cells: development and role in nerve repair. *Cold Spring Harb. Perspect. Biol.* **7**, a020487 (2015).
6. Svaren, J. & Meijer, D. The molecular machinery of myelin gene transcription in Schwann cells. *Glia* **56**, 1541–1551 (2008).
7. Feltri, M.L., Poitelon, Y. & Previtali, S.C. How Schwann cells sort axons: new concepts. *Neuroscientist* **22**, 252–265 (2015).
8. Halder, G., Dupont, S. & Piccolo, S. Transduction of mechanical and cytoskeletal cues by YAP and TAZ. *Nat. Rev. Mol. Cell Biol.* **13**, 591–600 (2012).
9. Taveggia, C. *et al.* Neuregulin-1 type III determines the ensheathment fate of axons. *Neuron* **47**, 681–694 (2005).
10. Engler, A.J., Sen, S., Sweeney, H.L. & Discher, D.E. Matrix elasticity directs stem cell lineage specification. *Cell* **126**, 677–689 (2006).
11. Reginensi, A. *et al.* Yap- and Cdc42-dependent nephrogenesis and morphogenesis during mouse kidney development. *PLoS Genet.* **9**, e1003380 (2013).
12. Feltri, M.L. *et al.* P0-Cre transgenic mice for inactivation of adhesion molecules in Schwann cells. *Ann. NY Acad. Sci.* **883**, 116–123 (1999).
13. Feltri, M.L. *et al.* Conditional disruption of β_1 integrin in Schwann cells impedes interactions with axons. *J. Cell Biol.* **156**, 199–209 (2002).
14. Benninger, Y. *et al.* Essential and distinct roles for Cdc42 and Rac1 in the regulation of Schwann cell biology during peripheral nervous system development. *J. Cell Biol.* **177**, 1051–1061 (2007).
15. Grinspan, J.B., Marchionni, M.A., Reeves, M., Coulaloglou, M. & Scherer, S.S. Axonal interactions regulate Schwann cell apoptosis in developing peripheral nerve: neuregulin receptors and the role of neuregulins. *J. Neurosci.* **16**, 6107–6118 (1996).
16. Vassilev, A., Kaneko, K.J., Shu, H., Zhao, Y. & DePamphilis, M.L. TEAD/TEF transcription factors utilize the activation domain of YAP65, a Src/Yes-associated protein localized in the cytoplasm. *Genes Dev.* **15**, 1229–1241 (2001).
17. Hung, H.A., Sun, G., Keles, S. & Svaren, J. Dynamic regulation of Schwann cell enhancers after peripheral nerve injury. *J. Biol. Chem.* **290**, 6937–6950 (2015).
18. Lopez-Anido, C. *et al.* Differential Sox10 genomic occupancy in myelinating glia. *Glia* **63**, 1897–1914 (2015).
19. Garratt, A.N., Voiculescu, O., Topilko, P., Charnay, P. & Birchmeier, C. A dual role of erbB2 in myelination and in expansion of the schwann cell precursor pool. *J. Cell Biol.* **148**, 1035–1046 (2000).
20. Guo, L., Moon, C., Zheng, Y. & Ratner, N. Cdc42 regulates Schwann cell radial sorting and myelin sheath folding through NF2/merlin-dependent and independent signaling. *Glia* **61**, 1906–1921 (2013).
21. Topilko, P. *et al.* Krox-20 controls myelination in the peripheral nervous system. *Nature* **371**, 796–799 (1994).
22. Kuhlbrodt, K., Herbarth, B., Sock, E., Hermans-Borgmeyer, I. & Wegner, M. Sox10, a novel transcriptional modulator in glial cells. *J. Neurosci.* **18**, 237–250 (1998).
23. Liu-Chittenden, Y. *et al.* Genetic and pharmacological disruption of the TEAD-YAP complex suppresses the oncogenic activity of YAP. *Genes Dev.* **26**, 1300–1305 (2012).
24. Pellegatta, M. *et al.* $\alpha_6\beta_1$ and $\alpha_7\beta_1$ integrins are required in Schwann cells to sort axons. *J. Neurosci.* **33**, 17995–18007 (2013).
25. Srinivasan, R. *et al.* Genome-wide analysis of EGR2/SOX10 binding in myelinating peripheral nerve. *Nucleic Acids Res.* **40**, 6449–6460 (2012).
26. Anbanandam, A. *et al.* Insights into transcription enhancer factor 1 (TEF-1) activity from the solution structure of the TEA domain. *Proc. Natl. Acad. Sci. USA* **103**, 17225–17230 (2006).
27. van der Flier, A. & Sonnenberg, A. Function and interactions of integrins. *Cell Tissue Res.* **305**, 285–298 (2001).
28. Previtali, S.C. *et al.* Expression of laminin receptors in Schwann cell differentiation: evidence for distinct roles. *J. Neurosci.* **23**, 5520–5530 (2003).
29. Berti, C. *et al.* Nonredundant function of dystroglycan and β_1 integrins in radial sorting of axons. *Development* **138**, 4025–4037 (2011).
30. Subramanian, A. *et al.* Gene set enrichment analysis: a knowledge-based approach for interpreting genome-wide expression profiles. *Proc. Natl. Acad. Sci. USA* **102**, 15545–15550 (2005).
31. Horton, J.D. *et al.* Combined analysis of oligonucleotide microarray data from transgenic and knockout mice identifies direct SREBP target genes. *Proc. Natl. Acad. Sci. USA* **100**, 12027–12032 (2003).
32. Leblanc, S.E. *et al.* Regulation of cholesterol/lipid biosynthetic genes by Egr2/Krox20 during peripheral nerve myelination. *J. Neurochem.* **93**, 737–748 (2005).

33. Le, N. *et al.* Analysis of congenital hypomyelinating Egr2Lo/Lo nerves identifies Sox2 as an inhibitor of Schwann cell differentiation and myelination. *Proc. Natl. Acad. Sci. USA* **102**, 2596–2601 (2005).
34. Chang, C. *et al.* A laminin 511 matrix is regulated by TAZ and functions as the ligand for the $\alpha_{6B}\beta_1$ integrin to sustain breast cancer stem cells. *Genes Dev.* **29**, 1–6 (2015).
35. Lopez-Fagundo, C., Bar-Kochba, E., Livi, L.L., Hoffman-Kim, D. & Franck, C. Three-dimensional traction forces of Schwann cells on compliant substrates. *J. R. Soc. Interface* **11**, 20140247 (2014).
36. Jagielska, A. *et al.* Mechanical environment modulates biological properties of oligodendrocyte progenitor cells. *Stem Cells Dev.* **21**, 2905–2914 (2012).
37. Irvine, K.D. & Harvey, K.F. Control of organ growth by patterning and Hippo signaling in *Drosophila*. *Cold Spring Harb. Perspect. Biol.* **7**, a019224 (2015).
38. Zanconato, F. *et al.* Genome-wide association between YAP/TAZ/TEAD and AP-1 at enhancers drives oncogenic growth. *Nat. Cell Biol.* **17**, 1218–1227 (2015).
39. Guo, L. & Teng, L. YAP/TAZ for cancer therapy: opportunities and challenges (review). *Int. J. Oncol.* **46**, 1444–1452 (2015).
40. Kim, M., Kim, T., Johnson, R.L. & Lim, D.S. Transcriptional co-repressor function of the Hippo pathway transducers YAP and TAZ. *Cell Rep.* **11**, 270–282 (2015).
41. Aragona, M. *et al.* A mechanical checkpoint controls multicellular growth through YAP/TAZ regulation by actin-processing factors. *Cell* **154**, 1047–1059 (2013).
42. Anliker, B. *et al.* Lysophosphatidic acid (LPA) and its receptor, LPA1, influence embryonic schwann cell migration, myelination, and cell-to-axon segregation. *Glia* **61**, 2009–2022 (2013).
43. Grigoryan, T. *et al.* Wnt/Rspondin/β-catenin signals control axonal sorting and lineage progression in Schwann cell development. *Proc. Natl. Acad. Sci. USA* **110**, 18174–18179 (2013).
44. Petersen, S.C. *et al.* The adhesion GPCR GPR126 has distinct, domain-dependent functions in Schwann cell development mediated by interaction with laminin-211. *Neuron* **85**, 755–769 (2015).
45. Chen, Z.L. & Strickland, S. Laminin γ1 is critical for Schwann cell differentiation, axon myelination, and regeneration in the peripheral nerve. *J. Cell Biol.* **163**, 889–899 (2003).
46. McKee, K.K. *et al.* Schwann cell myelination requires integration of laminin activities. *J. Cell Sci.* **125**, 4609–4619 (2012).
47. Grove, M. & Brophy, P.J. FAK is required for Schwann cell spreading on immature basal lamina to coordinate the radial sorting of peripheral axons with myelination. *J. Neurosci.* **34**, 13422–13434 (2014).
48. Schwartz, M.A. Integrins and extracellular matrix in mechanotransduction. *Cold Spring Harb. Perspect. Biol.* **2**, a005066 (2010).
49. Paavola, K.J., Sidik, H., Zuchero, J.B., Eckart, M. & Talbot, W.S. Type IV collagen is an activating ligand for the adhesion G protein-coupled receptor GPR126. *Sci. Signal.* **7**, ra76 (2014).
50. Chance, P.F. *et al.* DNA deletion associated with hereditary neuropathy with liability to pressure palsies. *Cell* **72**, 143–151 (1993).

ONLINE METHODS

Animal models and morphology. All experiments involving animals followed experimental protocols approved by the Roswell Park Cancer Institute, University at Buffalo, and the University of Wisconsin School of Veterinary Medicine Institutional Animal Care and Use Committees. *Taz*- and *Yap*-floxed mice in C57BL6/129 mixed background, and P0-Cre transgenic in the congenic C57BL6/N background were described previously[11,12]. The resulting mutant mice contained a mixed background, and only littermates were compared. Genotyping of mutant mice was performed by PCR on tail genomic DNA as described previously[11,12]. Mutant and control littermates were sacrificed at the indicated ages, and sciatic nerves were dissected. Males and females were included in the study. No animals were excluded from the study. Animals were housed in cages of 5 animals in 12/12-h light/dark cycles. Three animals per age and per genotype were analyzed, which is the minimum number required to obtain statistically significant results. Semithin section and electron microscopic analyses of sciatic nerves were performed as described[51]. For g-ratio (axon diameter/fiber diameter) and axonal distribution, 4 semithin images per sciatic nerve were acquired on a 100× objective. Axon and fiber diameters were quantified using the Leica QWin software (Leica Microsystem). Blinding was not possible because of the severity of the phenotype. Fibers were quantified using ImageJ (http://imagej.nih.gov). Data were analyzed using GraphPad Prism 6.01.

Cell culture. Primary rat Schwann cells were produced as described[52] and cultured in DMEM supplemented with 4.5 g l^{-1} glucose, L-glutamine, sodium pyruvate, 5% bovine growth serum, penicillin, streptomycin, 0.2% bovine pituitary extract, and 2 µM forskolin. Schwann cells were not used beyond the fourth passage. Rat DRG neurons were isolated from E14.5 embryos and established on collagen-coated glass coverslips as described[53]. Explants were cycled with fluoroxidine (FUDR, Sigma-Aldrich) to eliminate all non-neuronal cells. Neuronal medium was supplemented with 50 ng ml^{-1} NGF (Harlan, Bioproducts for Science). Rat Schwann cells were added (50,000 or 200,000 cells per cover slip) to establish myelinating cocultures of DRG neurons, and myelination was initiated by supplementing the medium with 50 µg ml^{-1} ascorbic acid (Sigma-Aldrich).

Western blotting and analysis. Sciatic nerves were dissected, stripped of the epineurium, frozen in liquid nitrogen, pulverized and resuspended in lysis buffer (95 mM NaCl, 25 mM Tris-HCl, pH 7.4, 10 mM EDTA, 2% SDS, 1 mM sodium orthovanadate, 1 mM NaF and 1:100 Protease Inhibitor Cocktail (Roche)). Protein lysates were incubated at 4 °C for 30 min then centrifuged at 16,000 rpm for 30 min at 4 °C. Supernatant protein concentrations were determined by BCA protein assay (Thermo Scientific) according to the manufacturer's instructions. Equal amounts of homogenates were diluted 3:1 in 4× Laemmli (250 mM Tris-HCl, pH 6.8, 8% SDS, 8% β-mercaptoethanol, 40% glycerol, 0.02% bromophenol blue), denatured 5 min at 100 °C, resolved on SDS–polyacrylamide gel, and electroblotted onto a PVDF membrane. Blots were then blocked with 5% BSA in 1× PBS, 0.05% Tween-20 and incubated overnight with the appropriate antibody. Antibodies were as follows: Abcam anti-ErbB2 1:250 (ab2428), BD Pharmingen anti-integrin β_1 subunit 1:200 (553715), Cell Signaling anti-Yap 1:1,000 (4912), Enzo anti-laminin α2 chain 1:200 (ALX-804-190), Novocastra anti-β-dystroglycan 1:50 (NCL-b-DG), Proteintech anti-Taz 1:1,000 (23306-1-AP), Santa Cruz anti-Cdc42 1:200 (sc-87), anti-integrin α_6 subunit 1:1,000 (sc-6597), anti-Yap 1:1,000 (sc-101199), Sigma-Aldrich anti-calnexin 1:3,000 (C4731), anti-Gapdh 1:2,000 (G9545) and anti-β-tubulin 1:2,000 (T4026). Anti-Egr2 1:200 was provided by D. Meijer, Centre for Neuroregeneration, Edinburg; anti-integrin α_7 subunit 1:1,000 was provided by G. Tarone, University of Turin[24]; anti-integrin β_4 subunit 1:1,000 was provided by P. Brophy, Centre for Neuroregeneration, Edinburgh; anti-laminin α5 chain 1:200 was gifted by L. Sorokin, University of Muenster[53]; anti-Sox10 1:200 was gifted by M. Wegner, FAU, Germany[18]. Membranes were then rinsed in 1× PBS and incubated for 1 h with secondary antibodies. Blots were developed using ECL, ECL plus (GE Healthcare) or Odyssey CLx infrared imaging system (Li-Cor). Western blots were quantified using Image J software (http://imagej.nih.gov/ij). Each experiment was performed at least two times on nerves from at least 3 animals.

TUNEL and proliferation assays. TUNEL and proliferation assays were performed on longitudinal sections of sciatic nerves. Slices were fixed with 4% PFA, permeabilized 1 min in methanol, blocked for 1 h in 20% FBS, 2% BSA, 0.1% Triton X-100 in PBS, and stained overnight with anti-rabbit PH3 antibody 1:400 (Millipore 06-576), followed by Jackson DyLight 488–conjugated secondary antibody. Slices were then incubated 15 min in TDT buffer (30 mM Tris, 140 mM sodium cacodylate trihydrate, 1 mM cobalt chloride) followed by enzyme mixture (60 U ml^{-1} TdT (Sigma-Aldrich), 6.25 mM Biotin-16-dUTP (Roche)) in TDT buffer for 1 h at 37 °C. The reaction was terminated with TB buffer (300 mM NaCl, 40 mM sodium citrate). After blocking in 2% BSA, coverslips were incubated with streptavidin–rhodamine secondary antibody. Nuclei were counterstained with DAPI and analyzed with fluorescence Leica DM6000B microscope. For longitudinal sections, nerves from 3 animals per genotype were analyzed. The proportion of p-H3 or TUNEL-positive nuclei were determined blindly from 5 random fields for each nerve. Stained nuclei were counted manually on images using ImageJ software. The total number of nuclei in sciatic nerves was obtained by measuring the total area of sciatic nerve over 400 µm of length and multiplying the total area by the nuclei density. Data were analyzed using Graphpad Prism 6.01.

Immunohistochemistry. Longitudinal sections and teased fibers from sciatic nerves were fixed in 4% PFA, permeabilized with acetone, washed in PBS, blocked for 1 h in 5% fish skin gelatin, 0.5% Triton X-100 in 1× PBS. Primary Schwann cells were fixed in 1% PFA, 0.5% DOTMAC; washed in PBS and blocked for 1 h in 5% NGS, 0.1% Triton in 1× PBS.

Co-cultures were fixed in 1% PFA, 0.5% DOTMAC, permeabilized with methanol, washed in PBS, and blocked for 1 h in 20% FCS, 1% BSA, 0.05% Triton in 1× PBS. The following primary antibodies were incubated overnight: Abcam anti-integrin β_4 subunit 1:150 (ab25254), BD Pharminogen anti-integrin β_1 subunit 1:150 (553837), Cell Signaling anti-Yap 1:100 (4912), Covance anti-NFH 1:700 (PCK-593P), anti-MBP 1:1,000 (SMI-99P), Enzo anti-laminin α2 chain 1:250 (ALX-804-190), Millipore ani-NFH 1:500 (AB1989), anti-α-dystroglycan IIH6 (05-593); and Proteintech anti-Yap/Taz 1:100 (23306-1-AP). Anti-integrin α_6 subunit 1:10 was provided by A. Sonnenberg, Netherlands Cancer Institute. Sections were rinsed in PBS, incubated 1 h with phalloidin-TRITC 1:100 (Sigma-Aldrich, P1951), Jackson DyLight 488 1:1,000, 549-conjugated 1:1,000 or 649-conjugated 1:1,000 secondary antibodies, stained with DAPI, and mounted with Vectashield (Vector Laboratories). Images were acquired with a Zeiss ApoTome or a confocal microscope Leica SP5II. Microscopy equipment and settings are detailed in **Supplementary Figure 5**. Maximum intensity projection from Z-stacks were created with Fiji software (fiji.sc). The localization of Yap amd Taz on various substrates and in the stretched experiment was assessed blindly.

Preparation of substrates of differing stiffness. Polyacrylamide (PA) gel and polydimethylsiloxane (PDMS) were used to create substrates with different elastic modulus (*E*) ranging from softer PA gel with E = 0.5 kPa and 40 kPa to stiff PDMS with E = 4 Mpa. The PA gels with two elastic moduli of 0.5 and 40 kPa were fabricated according to the protocol described by Tse *et al.*[54]. Briefly, 18-mm round coverslips were cleaned with 70% ethanol and treated with 0.1 M NaOH on a hot plate to create a uniform thin NaOH film on the surface. The surface was then coated with 3-aminopropyltriethoxysilane (TCI A0439) for 5 min followed by treatment with 0.5% glutaraldehyde (ACROS organics, 233280250) solution in PBS for 30 min. Functionalized coverslips were dried for gel coating. Acrylamide to Bis-acrylamide (BIO-RAD) ratio (v/v) of 3:0.1% and 8:0.48% were used to create 0.5- and 40-kPa PA gel substrates, respectively. After gel formation the gel surface was functionalized using sulfo-SANPAH (CovaChem, DF3363) by exposing to UV light. Finally, PA gels were coated with Poly-L-lysine (0.01 mg/ml) with or without laminin 211 (10 µg ml^{-1}, produced as described[53]. PDMS elastomer to curing agent (Sylgard 184) ratio of 4:1 was used to create PDMS substrate with 4 MPa elastic modulus as previously described by Zhao *et al.*[55]. Briefly, the elastomer and curing agent were mixed thoroughly and degassed, and a small amount of mixture was added to coverslips and spun to create a thin layer. The coverslips were then cured at 60 °C followed by 120 °C in the oven. Surface of the PDMS was coated using Poly-L-lysine with or without laminin at the concentrations previously mentioned. Schwann cells were trypsinized, counted and plated on the different substrates (glass, PA gel and PDMS) at 200,000 cells per coverslip. Cells were allowed to spread for 24 h before fixation.

Stretching experiment. Silicone sheets of 0.01 inch thickness (SMI silicone sheeting, 0.01-inch NRV G/G 40D, Saginaw, MI) were used for static stretching

doi:10.1038/nn.4316

experiment. The membrane was cut into 2.5-cm wide stripes and sterilized with 70% ethanol and under UV lamp. The surface was coated with PLL and laminin at aforementioned concentrations. The membranes were kept in PBS before use. Schwann cells were seeded on silicone sheet at 200,000 cells in a patterned area comparable to an 18-mm coverslip and were allowed to grow for 24 h. The membrane was then mounted on a custom-made uniaxial stretching device and stretched to 150% strain. The samples were kept under static strain for 30 min and then relaxed and fixed immediately. Non-stretched membrane with plated cells was used as a negative control.

Verteporfin treatment. Primary cells were treated with 2 or 10 μM verteporfin (Sigma-Aldrich SML0534). At 4 h after treatment, cells were stimulated with 20 ng μl^{-1} neuregulin-1 β isoform (heregulin-β 1, R&D Systems). RNA was harvested at 24 h after treatment, and cDNA was analyzed by RT-qPCR using the following primers:

18S (Forward: CGCCGCTAGAGGTGAAATTCT, Reverse: CGAACCTCCGACTTTCGTTCT),

ErbB2 (Forward: AGGTCTGGAGGGAACATCCT, Reverse: TGGGATGCATGTGTCTCAGT),

Cdc42 (Forward: GCTCTGGAGATGCGTTCATAG, Reverse: GAAGCAATATTGGCTGCCTTG),

Egr2 (Forward: GCACTCTGTGGCCCTAGAACA, Reverse: GGCTGAGATGGCTCGAGAAA),

Sox10 (Forward: CGAATTGGGCAAGGTCAAGA, Reverse: CACCGGGAACTTGTCATCGT),

Itga6 (Forward: CGAGAGATCAACGACGAGAAAC, Reverse: TCTTTCCTACACCCTCCTCTATG),

Dag1 (Forward: CTCCCAGGGTGTTTCAGACT, Reverse: TCAGAGCAACCAAGGTGACA).

The S16 rat Schwann cell line[56] was obtained from R. Quarles, cultured as described[52], and expresses relatively high levels of myelin genes[25].

RNA preparation and RT-qPCR. Sciatic nerves were dissected, stripped of epineurium, frozen in liquid nitrogen and pulverized. Total RNA was prepared from sciatic nerve or Schwann cells with TRIzol (Roche Diagnostic). 1 μg of RNA was reverse transcribed using Superscript III (Invitrogen). For each reaction, 5 μM of oligo$(dT)_{20}$ and 5 ng μl^{-1} random hexamers were used. Quantitative PCR were performed using the 20ng of cDNA combined with 1× FastStart Universal Probe Master (Roche Diagnostic). Data were analyzed using the threshold cycle (Ct) and $2(^{-\Delta\Delta}Ct)$ method. *Actb* gene was used as endogenous gene of reference and the average expression of control animals was set as the reference for normalizing the data. For data representation in **Figure 5b** and **Supplementary Figure 2c**, only one control animal was used for normalizing the data. The primers and probe used are the following:

18S (Forward: CTCAACACGGGAAACCTCAC, Reverse: CGCTCCACCAACTAAGAACG, Probe:#77),

Actb (Forward: AAGGCCAACCGTGAAAAGAT, Reverse: GTGGTACGACCAGAGGCATAC, Probe:#56),

Cdc42 (Forward: TGTTTCCGAAATGCAGACAA, Reverse: TGACTGCATAGTTGTCAAAAACAG, Probe:#9),

Dag1 (Forward: CTGCTGCTGCTCCCTTTC, Reverse: GCAGTGTTGAAAACCTTATCTTCC, Probe:#99),

ErbB2 (Forward: TGTGTGGACCTGGACGAAC, Reverse: TGCAATGATGAATGTCACTGG, Probe:#3),

Itga6 (Forward: CCTGAAAGAAAATACCAGACTCTCA, Reverse: GGAACGAAGAACGAGAGAGG, Probe:#99),

Itga7 (Forward: AGAAGGTGGAGCCTAGCACA, Reverse: GCTGAACACCACACACTTGG, Probe:#49),

Itgb1 (Forward: CAACCACAACAGCTGCTTCTAA, Reverse: TCAGCCCTCTTGAATTTTAATGT, Probe:#2),

Itgb4 (Forward: CTTGGTCGCCGTCTGGTA, Reverse: TCGAAGGACACTACCCCACT, Probe:#9).

Chromatin Immunoprecipitation (ChIP). ChIP was carried out as described previously[25,57] with the following antibodies: goat IgG (Santa Cruz Biotechnology, sc-2028), Sox10 (R&D, AF2864), and Tead1 (BD Biosciences, 610923). Primers used included the following:

Tekt3 +7.8kb (Forward: AATACCAGCAGATCCGGAAGAC, Reverse: TTGACTCGTTCTCCCAGGTTTT),

Itga6 −22.8kb (Forward: TGCTTCTGATAAGCCCCAAC, Reverse: AAGTCCCAGACACGTCCTTG),

Itga6 −20.6kb (Forward: TGGAGGCAGAAGGAGAAAAA, Reverse: AGGGGCCTGTTAGGAACACT),

Itga6 −16.2kb (Forward: GACTTGAGCTGTCTGCATGG, Reverse: TGGACTGACTAGGCTTCCACA),

Itga6 −8.5kb (Forward: AAAAGCCAAACAAACCCAGA, Reverse: GGCTAGGGCAAGCTAAGGAT),

Itga6 −7.8kb (Forward: TGCTTTTGGTCATGTGGTTG, Reverse: ACCACTGGCTAGCTCAGCAT),

Itga6 −165bp (Forward: TCGATAAAACGCCGGAGAGT, Reverse: GTAGCTAGCAGCCGCTCAAT),

Dag1 +3kb (Forward: ATGAACCCCTCTTCCTGACC, Reverse: CCTTGCTGAGACTGTGCTCA),

Dag1 −36kb (Forward: GGATGGAAGACTGAAAGGCC, Reverse: CCCTTTCCCTCTGGTGTGAG).

Bioinformatics. H3K27ac enrichment at select loci was obtained from previously published ChIP-seq data[18], and TEAD motifs were found using Homer[58].

RNA-seq analysis. Sciatic, trigeminal and brachial nerves at P3 were dissected, frozen in liquid nitrogen and pulverized. Total RNA was prepared from pools of nerves (8 trigeminal, 8 brachial and 8 sciatic nerves per pool) with TRIzol (Roche Diagnostic), then purified with RNeasy column (Qiagen). Samples were quantified using Ribogreen Assay (Invitrogen) and the quality of samples were checked using Agilent Bioanalyzer 2100 RNA nano 6000 chip (Agilent). Illumina TruSeq RNA sample preparation kit (Illumina) was used to prepare cDNA libraries from RNA samples. Samples were polyA selected to isolate mRNA, the mRNA was cleaved into fragments, the first strand reverse transcribed to cDNA using SuperScript II reverse Transcriptase (Invitrogen) and random primers, followed by second strand cDNA synthesis using Second Strand Master Mix supplied with the kit. After end repair, the addition of a single 'A' base, and ligation with adapters, the products were enriched and purified with PCR to create the final cDNA library as per manufacturer's protocol. cDNA libraries were quantified using Picogreen Assay (Invitrogen) and Library Quantification kit (Kapa Biosystems). Agilent Bioanalyzer 2100 DNA 7500 chip was used to confirm the quality and size of the cDNA libraries. The cDNA libraries were then normalized, pooled and paired-end sequenced (100 standard cycles) using the Illumina HiSeq 2500 following the manufacturer's instructions at the UB Genomics and Bioinformatics Core Facility (Buffalo, NY). Sequences were aligned to the UCSC Mm10 mouse genome using tophat (v2.0.13) and counts per gene determined using htseq (v0.6.1). R/Bioconductor was used for subsequent analysis. Following loading of read counts using DESeq, edgeR was used for differential expression analysis of read counts[59]. Genes with low counts (less than 1 count per million) in at least three libraries were removed from the analysis, and TMM normalization applied to account for differences between libraries. For differential expression analysis, common NB dispersion was estimated and a generalized linear model likelihood ratio test was used to determine differential expression between cKO and wild-type mice. *P* values were controlled for multiple testing by determining the false discovery rate (FDR). Pathway analysis was performed in edgeR using Gene Ontology (GO) enrichment analysis, KEGG pathway enrichment analysis, and gene set enrichment analysis of Broad C2 gene sets (v5) using roast. Heatmaps were plotted using $\log_2$(counts per million), with a prior count of 1.

Statistical analyses. Experiments were not randomized, but data collection and analysis were performed blindly to the conditions of the experiments. No data were excluded from the analyses. Data obtained were presented as mean ± s.e.m. or mean ± s.d. Two-tailed unpaired Student's *t*-test, two tailed unpaired Student's *t*-test with Bonferroni correction, Fisher's exact test, one-way ANOVA and two-way ANOVA were used for statistical analysis of the differences among multiple groups according to the number of samples. No statistical methods were used to predetermine sample sizes, but our sample sizes are similar those generally employed in the field. Data distribution was assumed to be normal, but this was not formally tested. $P < 0.05$ were

considered significant. *P* values, *t*-distributions and degrees of freedom (df) for **Figures 3–5** were as follows: **Figure 3**, *Taz* cKO–*Yap* cHet myelinated fibers, $P < 0.0001$, $t = 15.08$, df = 4; double cKO myelinated fibers, $P < 0.0001$, $t = 26.55$, df = 3; *Taz* cKO amyelinated fibers $P = 0.013$, $t = 6.261$, df = 4; *Yap* cKO amyelinated fibers $P = 0.0009$, $t = 13.1$, df = 4; *Taz* cKO–*Yap* cHet myelinated fibers $P = 0.011$, $t = 6.572$, df = 4; *Yap* cKO–*Taz* cHet myelinated fibers $P = 0.0068$, $t = 7.545$, df = 4. **Figure 4**, one-way ANOVA $P = 0.0003$, $F_{(2,10)} = 20.88$ with Bonferroni *post hoc* test; *Taz* cKO $P = 0.0325$; *Taz* cKO–*Yap* cHet myelinated fibers $P = 0.0001$ (**b**); TUNEL $P = 0.021$, $t = 1.461$, df = 4; p-H3 $P = 0.012$, $t = 4.341$, df = 4; two-tailed unpaired Student's *t* test (**d**). **Figure 5a**, one-way ANOVA $P < 0.0001$, $F_{(2,6)} = 228.9$ with Bonferroni *post hoc* test; *Dag1* 2 µM $P < 0.0001$; *Dag1* 10 µM $P < 0.0001$; *Itga6* 2 µM $P < 0.0001$; *Itga6* 10 µM $P < 0.0001$. **Figure 5b**, one-way ANOVA *Dag1* $P = 0.0263$; *Dag1* $F_{(2,6)} = 7.082$ with Bonferroni *post hoc* test; *Taz* cKO–*Yap* cHet $P = 0.0242$; one-way ANOVA *Itga6* $P = 0.0003$, $F_{(2,6)} = 42.47$ with Bonferroni *post hoc* test; *Taz* cKO $P = 0.0114$, *Taz* cKO–*Yap* cHet $P = 0.0002$. **Figure 5c**, two-way ANOVA $P < 0.0001$, $F_{(2,30)} = 28.79$ with Bonferroni *post hoc* test. Sox10 *Itga6* −20.6 kb $P < 0.0001$, Sox10 *Itga6* −165 bp $P = 0.0027$, Sox10 *Dag1* −3 kb $P = 0.0063$, Sox10 *Dag1* +36 kb $P = 0.0156$ 0.05, Tead1 *Itga6* −20.6 kb $P < 0.0001$, Tead1 *Dag1* +36 kb $P < 0.0001$. **Figure 5d**, two-way ANOVA $P = 0.0004$, $F_{(4,32)} = 9.947$ with Bonferroni *post hoc* test. *Dag1 Taz* cKO–*Yap* cHet $P = 0.006$, *Itga6 Taz* cKO $P = 0.0206$, *Itga6 Taz* cKO–*Yap* cHet $P < 0.0001$, *Itgb4 Taz* cKO $P = 0.011$, *Itgb4 Taz* cKO–*Yap* cHet $P = 0.0029$.

Data availability. The data supporting the findings of this study are available within the article and its supplementary information files. All original data are available from the corresponding author upon reasonable request.

A **Supplementary Methods Checklist** is available.

51. Quattrini, A. *et al.* Beta 4 integrin and other Schwann cell markers in axonal neuropathy. *Glia* **17**, 294–306 (1996).
52. Gokey, N.G., Srinivasan, R., Lopez-Anido, C., Krueger, C. & Svaren, J. Developmental regulation of microRNA expression in Schwann cells. *Mol. Cell. Biol.* **32**, 558–568 (2012).
53. Colombelli, C. *et al.* Perlecan is recruited by dystroglycan to nodes of Ranvier and binds the clustering molecule gliomedin. *J. Cell Biol.* **208**, 313–329 (2015).
54. Tse, J.R. & Engler, A.J. Preparation of hydrogel substrates with tunable mechanical properties. *Curr. Protoc. Cell Biol.* **10**, 10.16 (2010).
55. Zhao, R., Chen, C.S. & Reich, D.H. Force-driven evolution of mesoscale structure in engineered 3D microtissues and the modulation of tissue stiffening. *Biomaterials* **35**, 5056–5064 (2014).
56. Toda, K., Small, J.A., Goda, S. & Quarles, R.H. Biochemical and cellular properties of three immortalized Schwann cell lines expressing different levels of the myelin-associated glycoprotein. *J. Neurochem.* **63**, 1646–1657 (1994).
57. Jones, E.A. *et al.* Distal enhancers upstream of the Charcot-Marie-Tooth type 1A disease gene *PMP22*. *Hum. Mol. Genet.* **21**, 1581–1591 (2012).
58. Heinz, S. *et al.* Simple combinations of lineage-determining transcription factors prime *cis*-regulatory elements required for macrophage and B cell identities. *Mol. Cell* **38**, 576–589 (2010).
59. Robinson, M.D., McCarthy, D.J. & Smyth, G.K. edgeR: a Bioconductor package for differential expression analysis of digital gene expression data. *Bioinformatics* **26**, 139–140 (2010).